Monografías de la Real Academia de Ciencias de Zaragoza **31**, 217–236, (2009).

The shallow water model: The relevance of geometry and turbulence.

M. Elena Vázquez-Cendón[1], Luis Cea[2] and Jerónimo Puertas[2]

[1]Applied Mathematics Department
University of Santiago de Compostela. 15782 Santiago de Compostela, Spain

[2]Environmental and Water Engineering Group, Civil Engineering School
University of A Coruña, A Coruña, Spain

Abstract

The main goal of this contribution is to apply the depth averaged shallow water equations to several free surface flows in which the treatment of the geometry, introduced on the mathematical model by the source terms, and the turbulence modelling are of special interest (cf. Cea et al. [6]). The convective flux is discretised with either an hybrid scheme (first order in the water depth and second order in the unit discharge), or a fully second order scheme, both of them upwind Godunov's schemes based on Roe's average. In order to avoid spurious oscillations of the free surface when the bathymetry is irregular, an upwind discretisation of the bed slope source term with second order corrections is used. The $k-\varepsilon$ equations are solved with either an hybrid or a second order scheme. In all the numerical simulations the importance of using a second order upwind spatial discretisation has been checked. A first order scheme may give rather good predictions for the water depth, but it introduces too much numerical diffusion and therefore, it excessively smooths the velocity profiles. This is specially important when comparing different turbulence models, since the numerical diffusion introduced by a first order upwind scheme may be of the same order of magnitude as the turbulent diffusion.

Keywords: shallow water model, Godunov's schemes, source terms discretization, turbulent flows, dual mesh

Mathematics Subject Classification 2000: 14H30, 14D05, 20F36

1 Introduction

The two-dimensional character of a free surface flow is usually enforced by a horizontal length scale much larger than the vertical one, and by a velocity field quasi-homogeneous over the water depth. Under these conditions the 3D Reynolds averaged Navier-Stokes equations can be simplified in order to obtain the depth averaged shallow water equations. Here, the term *shallow* refers to a small ratio between the vertical and horizontal length scales. Shallow flows appear in many engineering applications, mainly in river and coastal engineering, but also in certain hydraulic structures like open channels or sedimentation tanks, just to cite some examples.

The modelling of turbulence in shallow water flows has not been treated so profusely as in other fluid dynamics areas. Some depth averaged turbulence models have been proposed for the 2D-SWE. Those models derive from well known RANS turbulence models, including somehow the effects of bed friction in the turbulence field. Special mention should be given to the depth averaged $k-\varepsilon$ model proposed by Rastogi and Rodi in 1978 [18], which was the first depth averaged two-equation eddy viscosity model, and it is still the most commonly used with the 2D-SWE when turbulent effects are included in the computation.

The main effect of turbulence is to diffuse the velocity field. This turbulent diffusion, which is a *physical* effect, is added in the solution to the *numerical* diffusion inherent to the upwind schemes which are used for solving hyperbolic equations. For this reason, when modelling turbulence, it is even more important to use high resolution schemes for the convective flux, in order to reduce the numerical diffusion to the minimum without numerical instabilities. A first order scheme, which might be suitable for some problems, should not be used when turbulent effects are significant, because the numerical diffusion might be of the same order or even larger than the turbulent diffusion. In this paper we use an hybrid second-order/first-order scheme (first order in the water depth and second order in the unit discharge). The hybrid scheme uses a second order discretisation for the two unit discharge components, whilst keeping a first order discretisation for the water depth. In such a way the numerical diffusion is considerably reduced, without a significant reduction on the numerical stability of the scheme. In order to avoid spurious oscillations of the free surface when the bathymetry is irregular, an upwind discretisation of the bed slope source term is used [11, 3].

In order to show the capabilities of depth averaged models in the computation of turbulent flows, a finite volume model has been used to compute the flow in a coastal estuary and in a vertical slot fishway. The estuary considered has extensive flat marsh areas which flood and dry periodically due to the tidal driven flow. This makes it possible to test the turbulence models in the presence of wet-dry fronts in complex two-dimensional

geometries with a very irregular bathimetry. The flow in the fishway is highly turbulent and it has strong recirculation eddies, which makes it a perfect test case for the turbulence models. All the numerical results are compared with extensive experimental data.

2 Mathematical model

This section presents some basic notions related to shallow water turbulent flows and the mathematical model used in this work.

2.1 2D Shallow water model

The mathematical derivation of the 2D-SWE can be found in many hydrodynamic books, and has already been presented by many authors. Minor differences appear from one derivation to another, but basically the process consists in assuming an hydrostatic pressure distribution, integrating the horizontal 3D Reynolds averaged Navier-Stokes equations over the water depth, applying Leibnitz's rule, and using the kinematic free surface and bed surface conditions. Several approximations are done through the mathematical derivation. As it is well know, the approximations made are summarised in the following: incompressible flow, hydrostatic pressure and homogeneous behaviour over the water depth. With the former approximations, the turbulent depth averaged shallow water equations are obtained as:

$$\frac{\partial h}{\partial t} + \frac{\partial h U_j}{\partial x_j} = 0 \tag{1}$$

$$\frac{\partial h U_i}{\partial t} + \frac{\partial h U_i U_j}{\partial x_j} = -gh\frac{\partial h}{\partial x_i} - gh\frac{\partial z_b}{\partial x_i} - \frac{\tau_{b,i}}{\rho} + \frac{\partial}{\partial x_j}\left(\nu h \frac{\partial U_i}{\partial x_j}\right) + \frac{\partial}{\partial x_j}\left(h\frac{\tau^e_{ij}}{\rho}\right), \quad i = 1,2$$

where the Einstein summation convention ($j = 1, 2$) is used with the notations that are detailed next: U_i, $i = 1, 2$ are the two componets of the depth averaged horizontal velocities*, h is the water depth, g is the gravity acceleration, z_b is the bed elevation, ρ is the density of water, ν is the kinematic viscosity of water, and $\tau_{b,i}$, $i = 1, 2$ are the two horizontal components of the bed friction stresses model with the Manning formula:

$$\frac{\tau_{b,i}}{\rho} = gh\frac{n^2|U|U_i}{h^{\frac{4}{3}}}, \quad i = 1, 2. \tag{2}$$

where n is the Manning coefficient. The depth averaged effective stress, τ^e_{ij}, adds the depth averaged viscous stresses τ^v_{ij} , the turbulent stresses $-\overline{u'_i u'_j}$ -or *Reynolds stresses*-

*This notation allows to apply the Einstein summation convention, that simplifies the description of the model, in other sections of the work also is used $U_x = U_1$, $U_y = U_2$, to denote the two horizontal components of the depth averaged horizontal velocities.

and the longitudinal and lateral dispersion stresses terms D_{ij} (Rastogi and Rodi, [18]):

$$\frac{\tau_{ij}^e}{\rho} = \frac{\tau_{ij}^v}{\rho} - \overline{u_i' u_j'} + D_{ij}, \quad i,j = 1,2 \tag{3}$$

Their relative importance respect to the convective and turbulent stress terms depends on the magnitude of the velocities $\overline{u}'$ and $\overline{v}'$. The viscous stress terms are obtained from the water kinetic viscosity ν as:

$$\frac{\tau_{ij}^v}{\rho} = \nu \left(\frac{\partial U_i}{\partial x_j} + \frac{\partial U_j}{\partial x_i} \right). \tag{4}$$

2.2 The $k-\varepsilon$ model of Rastogi and Rodi

The depth averaged horizontal Reynolds stresses $\overline{u'^2}, \overline{u'v'}, \overline{v'^2}$ appearing in the 2D-SWE need to be computed by means of a depth averaged turbulence model, which are usually derived from RANS turbulence models by introducing in some way the effects of bed friction and shallowness in the turbulence field. In the models based on the hypothesis of Boussinesq the Reynolds stresses are evaluated from the expression:

$$-\overline{u_i' u_j'} = \nu_t \left(\frac{\partial U_i}{\partial x_j} + \frac{\partial U_j}{\partial x_i} \right) - \frac{2}{3} k \delta_{ij}, \tag{5}$$

where ν_t is the eddy viscosity and k is the turbulent kinematic energy. The turbulence model provides turbulent viscosity to use it in previous expression.

As it is anticipated in the title of the subsection, in this work we only described to the equations of the model $k-\varepsilon$ averaged in depth[†]. In the version of the model of length of mixture for shallow water flows proposed by Rastogi and Rodi [18], the turbulent viscosity ν_t is calculated from the local characteristics of the flow by means of the following expression:

$$\nu_t = c_\mu \frac{k^2}{\varepsilon}, \tag{6}$$

where k is the turbulent kinetic energy, ε are the rate of turbulence dissipation, and c_μ is a constant with value c_μ =0.09. The model solves an equation of transport for each one of the variables k and ε, where it considers the production due to bed friction, the production by velocity and dissipation gradients and the convective transport. The equations describe that it are:

$$\begin{aligned} \frac{\partial hk}{\partial t} + \frac{\partial U_j hk}{\partial x_j} &= \frac{\partial}{\partial x_j} \left((\nu + \frac{\nu_t}{\sigma_k}) h \frac{\partial k}{\partial x_j} \right) + hP_k + hP_{kv} - h\varepsilon, \\ \frac{\partial h\varepsilon}{\partial t} + \frac{\partial U_j h\varepsilon}{\partial x_j} &= \frac{\partial}{\partial x_j} \left((\nu + \frac{\nu_t}{\sigma_\varepsilon}) h \frac{\partial \varepsilon}{\partial x_j} \right) + hc_{\varepsilon 1} \frac{\varepsilon}{k} P_k + hP_{\varepsilon v} - hc_{\varepsilon 2} \frac{\varepsilon^2}{k}. \end{aligned} \tag{7}$$

[†]Other models also considered by the authors can be seen in [6].

The terms that take part in the second members, and whose interpretation will be described briefly next, are:

$$P_k = 2\nu_t(S_{11}^2 + S_{22}^2 + 2S_{12}^2), \qquad S_{ij} = \frac{1}{2}\left(\frac{\partial U_i}{\partial x_j} + \frac{\partial U_j}{\partial x_i}\right) \quad i,j = 1,2\,,$$

$$P_{kv} = c_k \frac{u_f^3}{h}, \qquad c_k = \frac{1}{c_f^{1/2}}, \quad u_f^2 = c_f|\mathbf{U}|^2,$$

$$P_{\varepsilon v} = c_\varepsilon \frac{u_f^4}{h^2}, \qquad c_\varepsilon = 3.6\frac{c_{\varepsilon 2}c_\mu^{1/2}}{c_f^{3/4}},$$

$$c_\mu = 0.09 \quad c_{\varepsilon 1} = 1.44 \quad c_{\varepsilon 2} = 1.92 \quad \sigma_k = 1.0 \quad \sigma_\varepsilon = 1.31$$

where the term P_k accounts for the production of turbulent energy due to horizontal velocity gradients, and it has the same expression as in the 2D shallow water model. The source terms P_{kv} and $P_{\varepsilon v}$ are responsible for modelling the 3D turbulence generated by bed friction, where c_f is the bed friction coefficient. The five constants of the model $(c_\mu, c_{\varepsilon 1}, c_{\varepsilon 2}, \sigma_k, \sigma_\varepsilon)$ are assumed to have the same values as in the original $k-\varepsilon$ model.

The model $k-\varepsilon$ is a relatively sophisticated model. In shallow water turbulent flows it provides relatively good results, being one of the used models more in this topic when the turbulence level is important. However, its degree of complexity does not guarantee correct results in any type of flow. Like any model of turbulence, the results obtained with the model $k-\varepsilon$ must be analyzed and be valued of critical form.

3 Finite volume discretisation of the turbulent shallow water equations

The computations displayed in this article have been done using the code TURBILLON[‡], developed in the Group of Engineering of the Water and the Environment (GEAMA) of the Universidade of A Coruña in collaboration with the Universidade of Santiago de Compostela. The code solves the shallow water equations using a finite volume method for two-dimensional non-structured meshes. In the following a brief description of the numerical schemes used in TURBILLON is done. A more detailed description can be found in Cea et al. [6]. This section presents an unstructured finite volume model for solving the 2D-SWE and turbulence models presented in previous section. A comprehensive description of finite volume methods for fluid dynamics can be found in [14, 20].

The two-dimensional shallow water equations can be written in vectorial form as:

$$\frac{\partial \mathbf{w}}{\partial t} + \frac{\partial \mathbf{F_x}}{\partial x} + \frac{\partial \mathbf{F_y}}{\partial y} = \mathbf{S} + \mathbf{G} + \mathbf{D} \tag{8}$$

[‡] `http://turbillon2d.googlepages.com`

$$\mathbf{w} = \begin{pmatrix} h \\ q_x \\ q_y \end{pmatrix}, \qquad \mathbf{F_x} = \begin{pmatrix} q_x \\ \dfrac{q_x^2}{h} + \dfrac{gh^2}{2} \\ \dfrac{q_x q_y}{h} \end{pmatrix}, \qquad \mathbf{F_y} = \begin{pmatrix} q_y \\ \dfrac{q_x q_y}{h} \\ \dfrac{q_y^2}{h} + \dfrac{gh^2}{2} \end{pmatrix},$$

$$\mathbf{S} = \begin{pmatrix} 0 \\ -gh\dfrac{\partial z_b}{\partial x} \\ -gh\dfrac{\partial z_b}{\partial y} \end{pmatrix}, \qquad \mathbf{G} = \begin{pmatrix} 0 \\ -\dfrac{\tau_{b,x}}{\rho} \\ -\dfrac{\tau_{b,y}}{\rho} \end{pmatrix}, \qquad \mathbf{D} = \begin{pmatrix} 0 \\ \dfrac{\partial}{\partial x_j}\left(\nu_e h \dfrac{\partial U_x}{\partial x_j}\right) \\ \dfrac{\partial}{\partial x_j}\left(\nu_e h \dfrac{\partial U_y}{\partial x_j}\right) \end{pmatrix},$$

where $\mathbf{w}$ is the vector of the conservative unknowns, ν_e is the effective viscosity ($\nu_e = \nu + \nu_t$). The vectors $\mathbf{F_x}$ and $\mathbf{F_y}$ account for the convective flux. The vector $\mathbf{S}$ accounts for the bed slope, $\mathbf{G}$ for the bed friction, and $\mathbf{D}$ for the turbulent and viscous diffusion.

The discretisation of the spatial domain will be made with edge-type finite volumes, which were introduced by Bermúdez et al. in [2]. These kind of control volumes are generated from a previous triangulation of the numerical domain, as sketched in Figure 2. The nodes (N_i and N_j) are placed at the midpoint of the edges of the triangulation, and the cells C_i are built from the vertex and the barycentre of the triangles. The control volumes built in such a way have 4 faces except in the boundaries, where they have 3 faces. This approach permits an easy definition of the normal vector at the boundary faces, avoiding the indetermination which may appear in certain boundary nodes when using vertex-type control volumes in complex geometries [9].

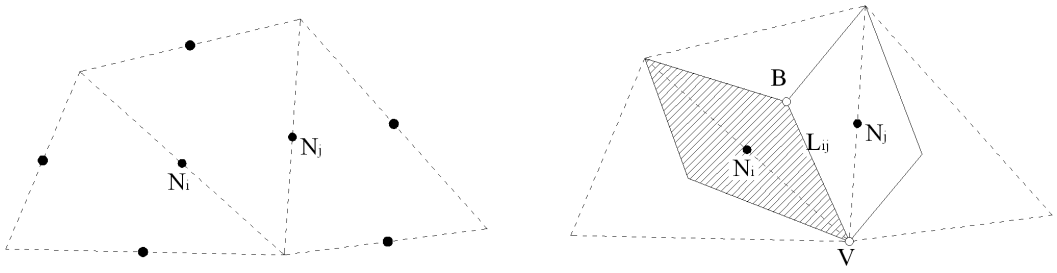

(a) Original triangular mesh. (b) Control volume C_i, defined by dashed region.

Figure 1.— Control volume generation from a triangular mesh

An explicit discretisation of Equation (8) is given by:

$$\frac{\mathbf{w}^{n+1} - \mathbf{w}^n}{\Delta t} + \frac{\partial \mathbf{F_x}}{\partial x}(\mathbf{w}^n) + \frac{\partial \mathbf{F_y}}{\partial y}(\mathbf{w}^n) = \mathbf{S}^n + \mathbf{G}^n + \mathbf{D}^n, \tag{9}$$

where the super-index n refers to time t^n. The extension of the scheme to second order in time can be easily implemented for example by a two-step method [5, 4]. Since the

solver is explicit in time, the time step is limited by the CFL condition, which has been implemented as:

$$\Delta t_i = \text{CFL} \min\left(\frac{d_i}{|\mathbf{U}|_i + \sqrt{g h_i}}\right), \tag{10}$$

where $d_i = A_i/P_i$ is the ratio between the area A_i and the perimeter P_i on each cell C_i. Integration of Equation (9) over a control volume or cell C_i and yields:

$$\frac{\mathbf{w}_i^{n+1} - \mathbf{w}_i^n}{\Delta t} A_i + \sum_{j \in K_i} \int_{L_{ij}} (\mathbf{F_x}\tilde{n}_x + \mathbf{F_y}\tilde{n}_y)\, dL = \int_{C_i} (\mathbf{S^n} + \mathbf{G^n} + \mathbf{D^n})\, dA \tag{11}$$

where $\mathbf{w}_i^n$ is the mean value of $\mathbf{w}$ in the cell C_i at time t^n, L_{ij} is the common face to the volumes C_i and C_j, $\tilde{\mathbf{n}} = (\tilde{n}_x, \tilde{n}_y)$ is the unit normal vector to the cell face, and K_i accounts for all the cells C_j which share any face with the cell C_i.

3.1 Convective flux

The convective flux in Equation (11) is discretised with a Roe upwind scheme [19]. Harten's regularisation [12] is applied when necessary. In order to obtain second order accuracy in space, the left and right states of the Riemann problem are obtained after a linear reconstruction of the variables $\mathbf{w}$ from the nodes to the cell faces, which can be computed as:

$$\mathbf{w}_{Ij} = \mathbf{w}_i + \frac{1}{2}\Delta_i^* \qquad\qquad \mathbf{w}_{iJ} = \mathbf{w}_j + \frac{1}{2}\Delta_j^* \tag{12}$$

where Δ_i^*, Δ_j^* are the limited slopes [21] at the nodes N_i and N_j, $\mathbf{w}_{Ij}$ is the extrapolated value of $\mathbf{w}_i$ to the cell face L_{ij}, and $\mathbf{w}_{iJ}$ is the extrapolated value of $\mathbf{w}_j$ to the cell face L_{ij} (Figure 2(b)). The limited slopes can be computed as:

$$\Delta_i^* = \begin{cases} \max[0,\, \min\left(\nabla \mathbf{w}_i \mathbf{r}_{ij},\, \Delta_{ij}\right)] & \text{if} \quad \Delta_{ij} > 0 \\ \min[0,\, \max\left(\nabla \mathbf{w}_i \mathbf{r}_{ij},\, \Delta_{ij}\right)] & \text{if} \quad \Delta_{ij} < 0 \end{cases}, \quad \text{with} \quad \Delta_{ij} = \mathbf{w}_j - \mathbf{w}_i \tag{13}$$

with an analogous expression for Δ_j^*. In (13) $\mathbf{r}_{ij}$ is the distance vector between the two nodes N_i and N_j. The triangles whose vertices are (N_i, N_{i_1}, N_{i_2}) and (N_j, N_{j_1}, N_{j_2}) know as *upwind triangles* see Figure 2(a) (more detail can be seen in Vázquez-Cendón [22]), and the gradients $\nabla \mathbf{w}_i$ and $\nabla \mathbf{w}_j$ are computed from the values of $\mathbf{w}$ at the nodes of the two upwind triangles respectively. The limited slopes computed from (13) reproduce the Minmod limiter [21].

The boundary integral of the convective flux in Equation (11) is approximated by the numerical flux $\boldsymbol{\phi}_{ij}$ as:

$$\int_{L_{ij}} (\mathbf{F_x}\tilde{n}_x + \mathbf{F_y}\tilde{n}_y)\, dL \approx \boldsymbol{\phi}_{ij}(\mathbf{w}_L, \mathbf{w}_R, \mathbf{n}_{ij}), \tag{14}$$

$$\begin{aligned} \boldsymbol{\phi}_{ij}(\mathbf{w}_L, \mathbf{w}_R, \mathbf{n}_{ij}) &= \frac{\mathbf{Z}(\mathbf{w}_L, \mathbf{n}_{ij}) + \mathbf{Z}(\mathbf{w}_R, \mathbf{n}_{ij})}{2} \\ &- \frac{1}{2}|\mathbf{Q}(\mathbf{w}_L, \mathbf{w}_R, \mathbf{n}_{ij})|(\mathbf{w}_R - \mathbf{w}_L), \end{aligned} \tag{15}$$

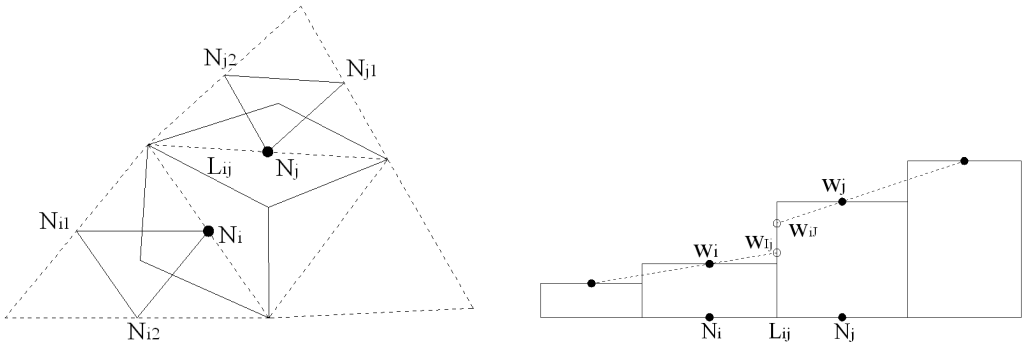

Figure 2.— Reconstruction of the conservative variables from the cell nodes to the faces. (a) *Upwind triangles*. (b) Linear reconstruction from nodes to faces, 1D view.

$$\mathbf{Z}(\mathbf{w}, \mathbf{n}_{ij}) = \mathbf{F_x}(\mathbf{w}) n_{ij_x} + \mathbf{F_y}(\mathbf{w}) n_{ij_y}, \quad |\mathbf{Q}| = \mathbf{X}|\mathbf{D}|\mathbf{X}^{-1}, \tag{16}$$

$$\mathbf{X} = \begin{pmatrix} 0 & 1 & 1 \\ -\tilde{n}_y & \tilde{U}_x + \tilde{c}\tilde{n}_x & \tilde{U}_x - \tilde{c}\tilde{n}_x \\ \tilde{n}_x & \tilde{U}_y + \tilde{c}\tilde{n}_y & \tilde{U}_y - \tilde{c}\tilde{n}_y \end{pmatrix}, \quad |\mathbf{D}| = \begin{pmatrix} |\tilde{\lambda}_1| & 0 & 0 \\ 0 & |\tilde{\lambda}_2| & 0 \\ 0 & 0 & |\tilde{\lambda}_3| \end{pmatrix} \tag{17}$$

$$\tilde{\lambda}_1 = n_x \tilde{U}_x + n_y \tilde{U}_y, \quad \tilde{\lambda}_2 = \tilde{\lambda}_1 + \tilde{c}\sqrt{n_x^2 + n_y^2}, \quad \tilde{\lambda}_3 = \tilde{\lambda}_1 - \tilde{c}\sqrt{n_x^2 + n_y^2}, \tag{18}$$

where $\mathbf{w}_L = \mathbf{w}_{Ij}$ and $\mathbf{w}_R = \mathbf{w}_{iJ}$ and $\mathbf{n}_{ij}$ is a normal vector to the cell face L_{ij} with the same length as the cell face.

3.2 Bed slope source term

When the upwind scheme given by Equations (12-18) is used with a centred discretisation of the bed slope source term $\mathbf{S}_i^C$, that is, $\mathbf{S}_i^C = \mathbf{S}(x_i, y_i, \mathbf{w}_i^n)$, spurious oscillations are generated under hydrostatic flow conditions. In order to avoid this unphysical oscillations, the bed slope source term must be discretised with an upwind scheme [2, 23, 11, 10]. A suitable upwind discretisation of $\mathbf{S}$ which is free of spurious oscillations when used with the first order scheme of Roe is given by [2, 10]:

$$\mathbf{S}_i = \mathbf{S}_i^C - \frac{1}{A_i} \sum_{j \in K_i} \frac{d_{\perp,ij}}{2} |\mathbf{n}_{ij}| |\mathbf{Q}|_{ij} \mathbf{Q}_{ij}^{-1} \tilde{\mathbf{S}}_{ij}, \tag{19}$$

$$\mathbf{S}_i^C = \frac{1}{A_i} \sum_{j \in K_i} \frac{d_{\perp,ij}}{2} |\mathbf{n}_{ij}| \tilde{\mathbf{S}}_{ij}, \quad \tilde{\mathbf{S}}_{ij} = -g \frac{h_i + h_j}{2} \frac{z_{b,j} - z_{b,i}}{d_{\perp,ij}} \begin{pmatrix} 0 \\ \tilde{n}_{x,ij} \\ \tilde{n}_{y,ij} \end{pmatrix},$$

where $\mathbf{S}_i$ is the upwind discretisation of the bed slope source term, $\tilde{\mathbf{S}}_{ij}$ is a centred approximation of the source term at the cell face L_{ij}, and $d_{\perp,ij} = \mathbf{r}_{ij} \tilde{\mathbf{n}}_{ij}$ is the projection of the distance between the nodes N_i and N_j (d_{ij}) on to the unit normal vector $\tilde{\mathbf{n}}_{ij}$.

Hubbard and García-Navarro [13] proposed a high order correction of the source term in order to obtain a fully second order scheme which gives an exact balance between convective flux and bed slope in the hydrostatic case.

All of the applications presented in this paper have been computed with both the hybrid scheme (first order for the water depth and second order for the unit discharges) as well as with the fully second order scheme. No significant differences have been found in the results given by both schemes, probably because the water depth gradients are not large enough. On the other hand, the hybrid scheme has been found to be much more stable than the fully second order scheme, especially when the bathymetry is irregular and there are unsteady wet-dry fronts in the solution.

3.2.1 Wet-dry fronts

A fixed finite volume mesh is used to discretise the whole spatial domain, and the control volumes are allowed to wet and dry during the simulation in order to model unsteady wet-dry fronts. A wet-dry tolerance parameter (ε_{wd}) is defined, such that if the water depth in a cell is lower than ε_{wd} the cell is considered to be dry. In the same way, if the water depth at the face L_{ij} is lower than ε_{wd}[§], the face is considered to be dry and it does not participate in the calculation. The water depth is never forced to be zero, in order to keep the mass conservation property of the scheme. The lowest value of ε_{wd} is desired in order to obtain accurate solutions. However, an excessively low value of ε_{wd} promotes numerical instabilities and necessitates the use of a very small CFL, especially when dealing with a very irregular bathymetry.

The fixed mesh approach needs a suitable wet-dry condition at the fluid interface which ensures the conservation of mass and momentum, and is at the same time not diffusive and free of spurious oscillations. Assuming a piecewise constant distribution of the bed elevation, two conditions are imposed at the wet-dry front: (1) redefinition of the bed elevation; (2) reflection condition.

The aim of redefining the bed elevation is to obtain an exact balance at the wet-dry front between the bed slope and the hydrostatic pressure term for hydrostatic conditions. As detailed by Brufau in [4], if the bed slope is not redefined spurious waves are generated at the front. If the wet-dry front occurs between the cells C_i and C_j, the modified bed slope at the front ($\Delta z_{b,ij}$) is defined as [4]:

$$\Delta z_{b,ij} = \begin{cases} h_i - h_j & \text{if} \quad h_j \leq \varepsilon_{wd} \quad \text{and} \quad h_i < z_{b,j} - z_{b,i} \\ z_{b,j} - z_{b,i} & \text{otherwise} \end{cases} \tag{20}$$

The treatment of the wet-dry fronts given by (20) gives the exact hydrostatic flow solution

[§]The wet-dry tolerance parameter is also used in the turbulence models.

Figure 3.— Wet-dry fronts. (a) Bed redefinition $\Delta z_{b,ij} = h_i$. Reflection condition $q_{n,ij} = 0$. (b) No redefinition. No reflection condition.

for any bed elevation without diffusing the front, and without generating any spurious oscillations of the free surface.

The reflection condition sets to zero the normal unit discharge at the cell face where the wet-dry front occurs ($q_{n,ij}$), which is the kinetic condition at a wall boundary:

$$q_{n,ij} = q_{x,ij}\tilde{n}_{x,ij} + q_{y,ij}\tilde{n}_{y,ij} = 0 \tag{21}$$

Condition (21) only applies when $h_i < z_{b,j} - z_{b,i}$ (Figure 3(a)). Setting the normal unit discharge to zero at the interface is justified by the assumption of a piecewise constant bed elevation, which is similar to a representation of the bed by a set of small vertical walls. In this way the wet-dry front is only allowed to advance when the water depth in the wet cell is larger than the bed step between cells ($h_i > z_{b,j} - z_{b,i}$, Figure 3(b)). It should be noticed that the unit discharge is not set to zero in the left cell C_i, but only at the face L_{ij} when computing the convective flux. Condition (21) also assures that the convective transport of k and ε at the wet-dry front is zero when $h_i < z_{b,j} - z_{b,i}$. In this case the diffusive flux of k and ε over the face L_{ij} is also set to zero.

3.3 Turbulent and viscous diffusion

The diffusion term is discretised with a semi-implicit centred scheme. In the following we will refer only to the x-momentum equation, with analogous expressions for the y-momentum equation. Integration of the diffusion term in the x-momentum equation over the cell C_i gives:

$$\begin{aligned} D_{tot} &= \int_{C_i} \frac{\partial}{\partial x}\left(\nu_e h \frac{\partial U_x}{\partial x}\right) + \frac{\partial}{\partial y}\left(\nu_e h \frac{\partial U_x}{\partial y}\right) dA \\ &\approx \sum_{j \in K_i} \nu_{e,ij} h_{ij} \left(\frac{\partial U_x}{\partial x} n_x + \frac{\partial U_x}{\partial y} n_y\right)_{ij} . \end{aligned} \tag{22}$$

When the eddy viscosity is large, it is convenient to implicit the main diagonal of the diffusion source term in order to relax the stability condition over the time step. In order to do so, following the ideas of Davidson [7], the total diffusive flux (D_{tot}) is split

in two parts: an orthogonal diffusion ($D_\perp$) and a non-orthogonal diffusion ($D_\parallel$), so that $D_{tot} = D_\perp + D_\parallel$.

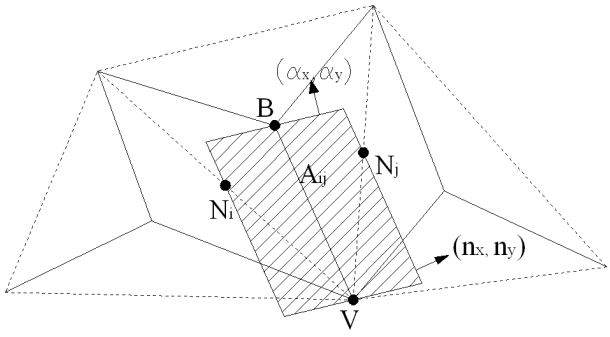

Figure 4.— Discretisation of the diffusion term.

The gradient of the velocity at the cell face L_{ij} is computed applying the Gauss theorem on the volume A_{ij}, which is defined by the shaded area in Figure 4. The two edges of the volume A_{ij} which pass through the nodes N_i and N_j are defined by the same normal vector as the cell face L_{ij}, i.e. $\mathbf{n}_{ij}$. The other two edges are parallel to the line which joins the nodes N_i and N_j, and are defined by the normal vector $\boldsymbol{\alpha}_{ij}$, with modulus $|\boldsymbol{\alpha}_{ij}| = |\mathbf{r}_{ij}|$, so that $\boldsymbol{\alpha}_{ij}\mathbf{r}_{ij} = 0$. The area of the volume is given by $A_{ij} = |\mathbf{n}_{ij}|d_{\perp,ij} = \mathbf{r}_{ij}\mathbf{n}_{ij}$. With these definitions, the gradient of U_x at the cell face L_{ij} is evaluated as:

$$\begin{aligned} \left.\frac{\partial U_x}{\partial x}\right|_{ij} &\approx \frac{1}{A_{ij}}\int_{A_{ij}} \frac{\partial U_x}{\partial x}\, dA = \frac{1}{A_{ij}}\int_L U_x \tilde{n}_x\, dL \\ &\approx \frac{1}{A_{ij}}\left(U_{x,j}n_{x,ij} + U_{x,B}\alpha_{x,ij} - U_{x,i}n_{x,ij} - U_{x,V}\alpha_{x,ij}\right) \end{aligned} \tag{23}$$

with an analogous expression for $\left.\dfrac{\partial U_x}{\partial y}\right|_{ij}$. The following expression is obtained for the discrete diffusive flux at the cell C_i:

$$\begin{aligned} D_{tot} &\approx \underbrace{\sum_{j\in K_i} \nu_{e,ij} h_{ij} \frac{|\mathbf{n}_{ij}|}{d_{\perp,ij}} \left(U_{x,j} - U_{x,i}\right)}_{D_\perp \equiv \text{orthogonal}} \\ &+ \underbrace{\sum_{j\in K_i} \nu_{e,ij} h_{ij} \frac{d_{ij}}{d_{\perp,ij}} \left(U_{x,B} - U_{x,V}\right)\left(\tilde{\alpha}_{x,ij}\tilde{n}_{x,ij} + \tilde{\alpha}_{y,ij}\tilde{n}_{y,ij}\right)}_{D_\parallel \equiv \text{non-orthogonal}} \end{aligned} \tag{24}$$

The non-orthogonal part ($D_{||}$) is treated explicitly with the rest of source terms, while the orthogonal part ($D_\perp$) is split as:

$$D_{\perp,ij} = \nu_{e,ij} h_{ij} \frac{|\mathbf{n}_{ij}|}{d_{\perp,ij}}(U_{x,j} - U_{x,i}) = \Gamma_{D_{\perp,ij}} U_{x,j} - \frac{\Gamma_{D_{\perp,ij}}}{h_i} q_{x,i} \tag{25}$$

where $\Gamma_{D_{\perp,ij}} = \dfrac{\nu_{e,ij} h_{ij} |\mathbf{n}_{ij}|}{d_{\perp,ij}}$ is the orthogonal diffusion coefficient. In Equation (25) all the variables are evaluated at time t^n except the unit discharge $q_{x,i}$, which is evaluated at time t^{n+1}. In this way no additional computational cost is introduced, since there is no need to solve any system of equations. In orthogonal meshes the vectors $\mathbf{n}_{ij}$ and $\boldsymbol{\alpha}_{ij}$ are perpendicular and therefore, the non-orthogonal diffusion in Equation (24) vanishes ($D_{\parallel} = 0$).

3.4 Discretisation of the $k - \varepsilon$ equations

The modelled $k - \varepsilon$ equations are written in vectorial form as:

$$\frac{\partial \boldsymbol{\Phi}}{\partial t} + \frac{\partial \mathbf{F}_{\boldsymbol{\Phi},\mathbf{x}}}{\partial x} + \frac{\partial \mathbf{F}_{\boldsymbol{\Phi},\mathbf{y}}}{\partial y} = \sum_{\mathrm{m}=1}^{4} \mathbf{H}_{\mathbf{m}} \tag{26}$$

$$\boldsymbol{\Phi} = \begin{pmatrix} hk \\ h\varepsilon \end{pmatrix}, \quad \mathbf{F}_{\boldsymbol{\Phi},\mathbf{x}} = \begin{pmatrix} hkU_x \\ h\varepsilon U_x \end{pmatrix} = U_x \boldsymbol{\Phi}, \quad \mathbf{F}_{\boldsymbol{\Phi},\mathbf{y}} = \begin{pmatrix} hkU_y \\ h\varepsilon U_y \end{pmatrix} = U_y \boldsymbol{\Phi}$$

$$\mathbf{H_1} = \begin{pmatrix} \dfrac{\partial}{\partial x_j}\left((\nu + \dfrac{\nu_t}{\sigma_k}) h \dfrac{\partial k}{\partial x_j}\right) \\ \dfrac{\partial}{\partial x_j}\left((\nu + \dfrac{\nu_t}{\sigma_\varepsilon}) h \dfrac{\partial \varepsilon}{\partial x_j}\right) \end{pmatrix}, \qquad \mathbf{H_2} = \begin{pmatrix} \min\left(2\nu_t S_{ij} S_{ij} h, 10\varepsilon h\right) \\ c_{1\varepsilon} \dfrac{\varepsilon}{k} 2\nu_t S_{ij} S_{ij} h \end{pmatrix},$$

$$\mathbf{H_3} = \begin{pmatrix} \min(c_k u_f^3, 10\varepsilon h) \\ c_\varepsilon \dfrac{u_f^4}{h} \end{pmatrix}, \qquad \mathbf{H_4} = \begin{pmatrix} -\varepsilon h \\ -c_{2\varepsilon} \dfrac{\varepsilon^2}{k} h \end{pmatrix}.$$

The source terms $\mathbf{H_m}$ (m=1,4) account respectively for the viscous and turbulent diffusion ($\mathbf{H_1}$), the production due to horizontal velocity gradients ($\mathbf{H_2}$), the production due to bed friction ($\mathbf{H_3}$), and the dissipation rate ($\mathbf{H_4}$). The same second order discretisation scheme described for the mean flow equations is used for the $k-\varepsilon$ equations. However, in this case the normal convective flux to the face L_{ij} ($\mathbf{Z}_{\boldsymbol{\Phi},ij}$) depends linearly on the depth averaged velocity as:

$$\mathbf{Z}_{\boldsymbol{\Phi},ij} = (U_x \tilde{n}_x + U_y \tilde{n}_y)_{ij} \boldsymbol{\Phi}_{ij} = U_{n,ij} \boldsymbol{\Phi}_{ij}. \tag{27}$$

At each cell face the numerical flux $\mathbf{Z}^*_{\boldsymbol{\Phi},ij}$ is computed as:

$$\mathbf{Z}^*_{\boldsymbol{\Phi},ij} = U_{n,ij} \frac{\boldsymbol{\Phi}_{Ij} + \boldsymbol{\Phi}_{iJ}}{2} - \frac{1}{2} |U_{n,ij}| \left(\boldsymbol{\Phi}_{iJ} - \boldsymbol{\Phi}_{Ij}\right), \tag{28}$$

where $U_{n,ij}$ is a centred discretisation of the normal velocity to the cell face, and $\boldsymbol{\Phi}_{iJ}, \boldsymbol{\Phi}_{Ij}$ are linearly extrapolated values from the cell nodes to the cell faces using (12).

All the source terms are discretised at the cell nodes using a centred scheme. In order to reinforce the stability of the scheme and to help the turbulent quantities k and ε to

remain positive during the computation, the following semi-implicit linearization of the source terms is used in the solver [7]:

$$\mathbf{H} = \mathbf{H}_N^n \mathbf{\Phi}^{n+1} + \mathbf{H}_P^n. \tag{29}$$

All the negative source terms are discretised in the form $\mathbf{H}_N^n \mathbf{\Phi}^{n+1}$, while the positive source terms are included in $\mathbf{H}_P^n$. The production source terms $\mathbf{H}_2$ and $\mathbf{H}_3$ are always positive and therefore, they are included in $\mathbf{H}_P^n$. The dissipation source term $\mathbf{H}_4$ is always negative, so it is discretised as:

$$\mathbf{H}_4 = \begin{pmatrix} -\varepsilon h \\ -c_{2\varepsilon}\dfrac{\varepsilon^2}{k} h \end{pmatrix} = \begin{pmatrix} -\left(\dfrac{\varepsilon}{k}\right)^n (kh)^{n+1} \\ -c_{2\varepsilon}\left(\dfrac{\varepsilon}{k}\right)^n (\varepsilon h)^{n+1} \end{pmatrix}. \tag{30}$$

The diffusion term $\mathbf{H}_1$ can be positive or negative and thus, it is included in $\mathbf{H}_P^n$ or $\mathbf{H}_N^n \mathbf{\Phi}^{n+1}$ depending on its sign. With these considerations the terms $\mathbf{H}_N^n$ and $\mathbf{H}_P^n$ in (29) are given by:

$$\mathbf{H}_N^n = \min\left(\frac{\mathbf{H}_1}{\mathbf{\Phi}}, 0\right)^n + \begin{pmatrix} -\dfrac{\varepsilon}{k} \\ -c_{2\varepsilon}\dfrac{\varepsilon}{k} \end{pmatrix}^n, \quad \mathbf{H}_P^n = \max\left(\mathbf{H}_1, 0\right)^n + \mathbf{H}_2^n + \mathbf{H}_3^n. \tag{31}$$

4 Applications

4.1 Tidal flow in the Crouch estuary

The Crouch estuary, Essex, UK (Figure 5), is a challenging test case if we consider its complex bathymetry, with extensive intertidal flats. The tidal range is approximately 4.8 m at the mouth. The maximum depth is about 15 m at high tides. Freshwater influx is negligible in the whole estuary, and therefore, all the water in the estuary is salt water. The large separation between horizontal and vertical length scales justify the use of a 2D-SWE model.

The flow in the model is completely driven by the water surface elevation at the mouth, which is the only open boundary condition to be imposed. The rest of the boundaries are treated as walls. Due to the size and complexity of the computational domain (27.65 Km^2) the mesh size near the walls is relatively coarse and therefore, a slip condition has been used at the wall boundaries. Accordingly, the normal velocity as well as the diffusion of k and ε are set to zero at the boundary faces. Nonetheless, most of the time during the simulation the wall boundaries are dry and thus, they do not participate in the solution. On the other hand the wet-dry front, which defines the fluid extension, plays a more important role in the flow field.

The water surface elevation at the mouth is directly obtained from a tidal gauge. The flow at the mouth is always subcritical. Hence, only the water depth needs to be imposed

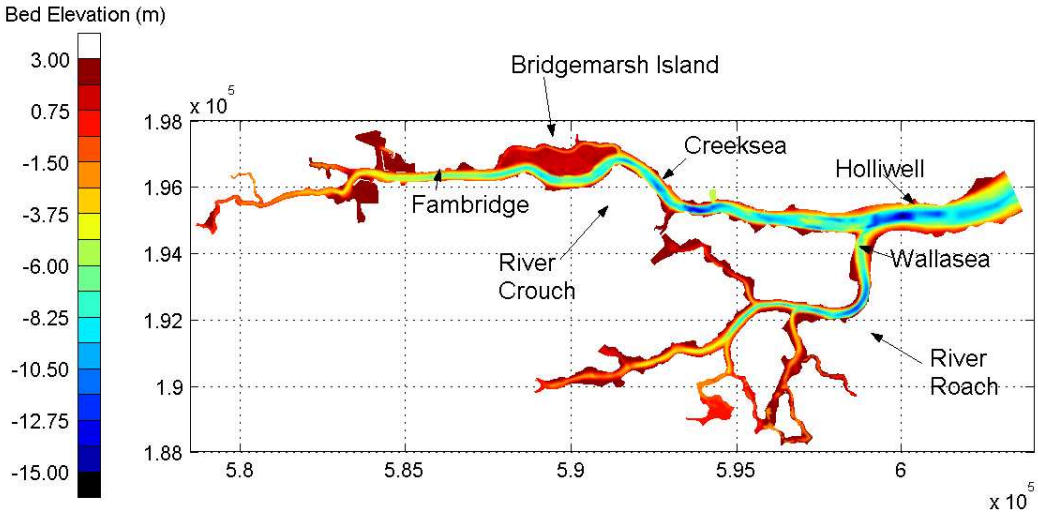

Figure 5.— Bathymetry of the Crouch-Roach estuary for the numerical model, relative to mean sea level at the mouth. Locations of tide gauges and current meter deployments are shown.

during the ebb tide (subcritical outlet). During the flood tide (subcritical inlet) the flow is forced to be perpendicular to the boundary, as an additional condition to the imposed water depth.

A Manning coefficient of $n = 0.02$ ms$^{-1/3}$ was used in the inter-tidal and sub-tidal regions, where the bottom sediments are predominantly muddy. There are also several marsh regions, which are assigned $n = 0.05$ ms$^{-1/3}$.

After using several meshes with different resolution, a mesh with approximately 50000 volumes was chosen. The numerical mesh used covers the whole estuary using 48995 control volumes. The area of the control volumes in the main channel is about 300 m^2.

The hybrid scheme was used in the computations, which proved to be much more stable than the fully second order scheme, while producing almost identical results.

The velocity field in the whole estuary is very dependent on the bathymetry, with velocities being highest in the deepest regions of the estuary. The sensitivity of the numerical results to the bed friction coefficient and turbulence model is much smaller than the differences between numerical and experimental data (see Cea et al. [6]). Some of the disagreements between numerical and experimental results are probably due to errors in the local bathymetry of the model. The fact of comparing the experimental velocity measured at a fixed height of 2 m above the bed, with the numerical depth-averaged velocity, might also account for some of these discrepancies.

In general water depth is rather well predicted by the model except at Fambridge, this is the reason beacuse we choose Figure 6 between all the numerical results showed in Cea [5] , where the tidal amplitude is slightly underpredicted. Regarding the current

speed, both ebb and flood flows are well predicted, although the maximum ebb velocity is slightly underpredicted at Fambridge. Figure 6 shows several numerical and experimental time-series for water depth and current speed.

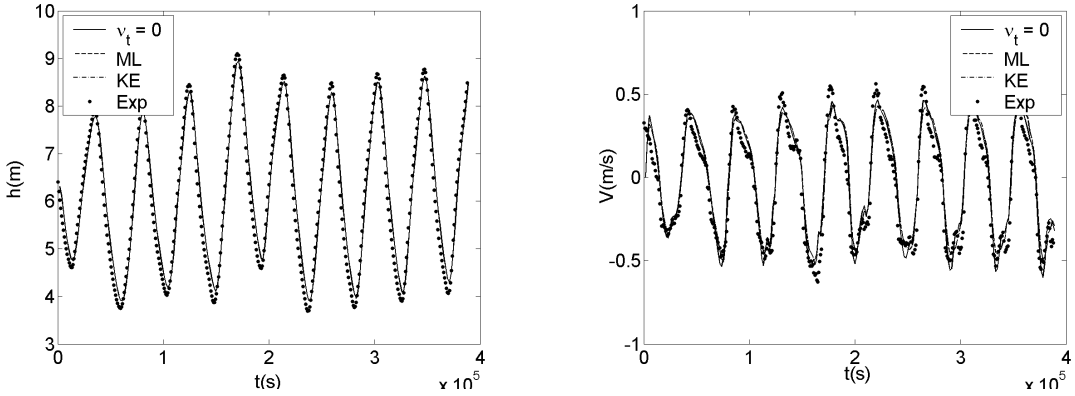

Figure 6.— Water depth and horizontal velocity time series at Fambridge. ML and $k-\varepsilon$ turbulence models, and zero eddy viscosity ($\nu_t = 0$).

In this case turbulence is mainly produced by bed friction(Figure 7). For uniform channel flow the eddy viscosity given by the $k-\varepsilon$ model reduces to $\nu_t^{k-\varepsilon} = 0.08 u_f h$, while the depth averaged mixing length model (ML) (see Cea et al. [6]) gives $\nu_t^{ML} = 0.068 u_f h$. For this reason the velocity and water depth fields are very insensitive to the turbulence model used.

Even in the mouth of the estuary, where the turbulence intensities are highest (Figure 7), the turbulent horizontal Reynolds number is rather large ($R_t = UL/\nu_t \approx 21000$). This means that the turbulent diffusion forces are small when compared to the convective forces, which diminishes the influence of the turbulence model on the mean velocity field. Velocity and water depth fields independent of the turbulence model were also obtained by Babarutsi et al. [1] when modelling shallow recirculating flows dominated by bed friction, by Davies et al. [8] when computing the tidal flow in the Irish Sea, and by Lloyd and Stansby [15] when modelling the flow around conical islands.

4.2 Turbulent flow in a vertical slot fishway

A vertical slot fishway is a channel divided into several pools separated by vertical slots through which the water flows downstream. Although the geometry of a vertical slot fishway is two-dimensional, the ratio between the water depth and the length of the pool is of the order of 0.5, and therefore, it is not straightforward that the 2D-SWE are able to reproduce the flow pattern in a vertical slot fishway. In fact, the hypotheses which are made in the derivation of the 2D-SWE are broken in some regions of the flow, specially near the slot. However, the numerical and experimental data agree quite well.

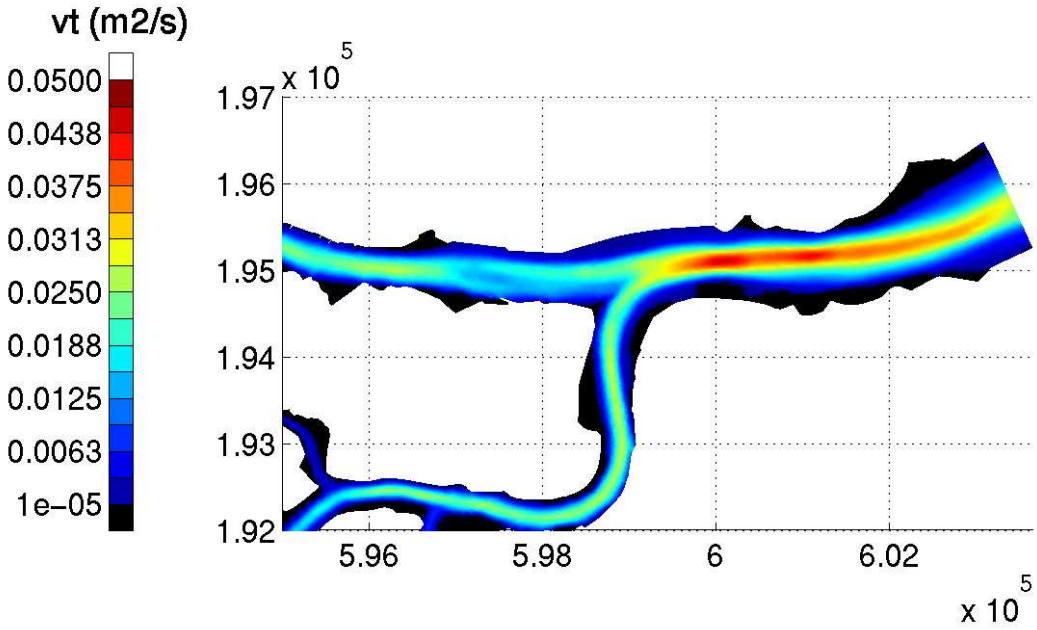

Figure 7.— Eddy viscosity field at the mouth of the estuary. Ebb tide. $k-\varepsilon$ model. Dry regions are shown in black.

From the experimental results of several researchers [17, 16] it follows that for uniform flow conditions the velocity field in vertical slot fishways is almost independent of the total flow discharge. On the other hand, the water depth is proportional to the flow discharge with an almost linear relation. The first feature we should expect from the numerical model is to reproduce this behaviour. In order to prove so, three different discharges covering almost the full range of experimental flow conditions were used in the simulations: 35 l/s and 105 l/s.

The flow pattern in the pools can be described as a main jet which crosses the pool from the inlet to the outlet slot. At each side of the jet a recirculation eddy appears. The flow separates behind the inlet slot baffle and the so-called lower eddy appears. Going through the outlet slot the flow is forced to reattach. Both eddies are driven by turbulent shear stress, and therefore their prediction is very dependent on the turbulence model used. The $k-\varepsilon$ model predicts maximum velocity and recirculation regions which are quite insensitive to the total discharge (Figure 8). This result is in direct agreement with the experimental data.

A comparison of the depth averaged longitudinal velocity at several cross sections reveals a quite satisfactory agreement between the experimental and numerical results (Figure 9).

The $k-\varepsilon$ model fails to predict the anisotropy between the two horizontal Reynolds stresses, and gives excessively large values of the transversal component $\overline{v'^2}$ (see Cea et al. [6]). Nonetheless, the global agreement between the experimental and numerical

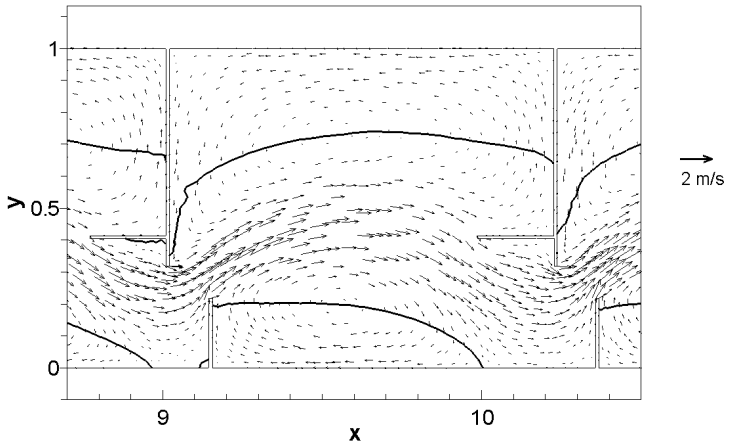

Figure 8.— Depth averaged velocity field. $Q = 105l/s$.The black line separates the regions with positive and negative longitudinal velocity

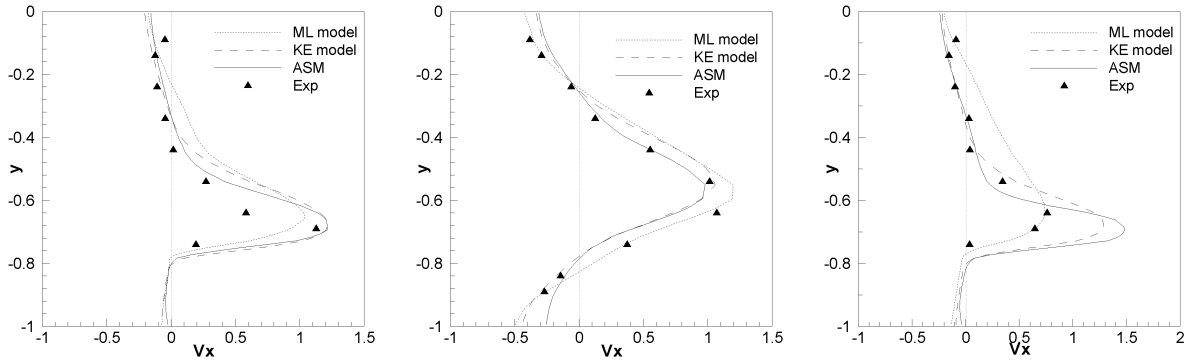

Figure 9.— Numerical and experimental depth averaged longitudinal velocity $V_x(m/s)$ at several cross sections. (a) $Q = 35$ l/s. x =0.16 m. (b) Q =35 l/s. x =0.46 m. (c) $Q = 105$ l/s. $x = 0.16$m

normal Reynolds stresses is quite satisfactory. The largest differences appear in the main jet stream, where the ASM tends to underpredict the turbulent energy, while the $k - \varepsilon$ model overpredicts it. The excessively large turbulence level given by the $k-\varepsilon$ model just downstream the inlet slot might be explained by the strong shear strain, with velocity gradients of the order of 20 s^{-1}. The flow conditions in this region, with a very strong swirl, as well as separation and reattachment in a very short distance, are beyond the capabilities of the eddy viscosity turbulence models. The largest source of turbulence in the pool is due to the strong shear strain in the inlet slot and lower eddy. The maximum value of the turbulent kinetic energy given by the $k - \varepsilon$ model is inside the eddy region, with values around 0.24 m^2/s^2.

5 Conclusions

In this paper we have presented a comprehensive study on depth averaged turbulence modelling on shallow flows, including a critical description of the equations and numerical schemes used to solve them, practical applications and experimental validation.

In order to avoid spurious oscillations when the bathimetry is irregular, an upwind discretisation of the bed slope term has been described. Alternatively to a fully second order scheme, we have described a rather simple, free of spurious oscillations and stable scheme, which reduces the numerical diffusion in a significant way, which just uses a second order discretisation for the two unit discharge components, whilst keeping a first order discretisation for the water depth and bed elevation. The resulting hybrid scheme has been used in the practical applications, giving accurate and stable results. Nevertheless, it is important to remark that the water depth gradient in all the applications was quite smooth.

It turned up that, even if the flow is fully turbulent in all the applications, the importance of the turbulence modelling is much dependent on the problem, to the point that in the Crouch estuary turbulence has not importance at all in the global flow field, while in the fishway its role is critical. Still, it should be remarked that the turbulence field might be important in order to compute sediment transport or dispersion of pollutants, which are problems usually dominated by turbulent diffusion.

The comparison between the numerical and experimental results in the applications presented in section 4 showed that the depth averaged shallow water equations, coupled with a suitable turbulence model, may be used in order to compute the free surface flow in vertical slot fishways as well as the tidal flow in complex estuaries with extensive tidal flats. The importance of a correct turbulence modelling in the fishway was confirmed by the numerical results. The $k - \varepsilon$ model give fairly accurate velocity fields.

References

[1] S. Babarutsi, M. Nassiri, and V.H. Chu. Computation of shallow recirculating flow dominated by friction. *J. Hydraul. Eng.*, 122(7):367–372, 1996.

[2] A. Bermúdez, A. Dervieux, J.A. Desideri, and M.E. Vázquez-Cendón. Upwind schemes for the two-dimensional shallow water equations with variable depth using unstructured meshes. *Comput. Methods Appl. Mech. Eng.*, 155:49–72, 1998.

[3] A. Bermúdez and M.E. Vázquez-Cendón. Upwind methods for hyperbolic conservation laws with source terms. *Comput. Fluids*, 23(8):1049–1071, 1994.

[4] P. Brufau. Simulación bidimensional de flujos hidrodinámicos transitorios en geometrías irregulares. Tesis doctoral. Área de Mécanica de Fluidos. Universidad de Zaragoza, 2000.

[5] L. Cea. An unstructured finite volume model for unsteady turbulent shallow water flow with wet-dry fronts: Numerical solver and experimental validation. Doctoral Thesis. Departamento de Métodos Matemáticos y de Representación. Universidad de A Coruña, 2005.

[6] L. Cea, J. Puertas, and M.E. Vázquez-Cendón. Depth averaged modelling of turbulent shallow water flow with wet-dry fronts. *Archives of Computational Methods in Engineering*, 14(3):303–341, 2007.

[7] L. Davidson. Implementation of a $k-\varepsilon$ model and a Reynolds Stress Model into a multi-block code. Technical Report CRS4-APPMATH-93-21, Aplied Mathematics and Simulation Group CRS4, Cagliary, Italy, 1993.

[8] A M. Davies, J E. Jones, and J. Xing. Review of recent developments in tidal hydrodynamic modeling. II: Turbulence energy models. *J. Hydraul. Eng.*, 123(4):278–292, 1997.

[9] A. Dervieux and J.A. Desideri. Compressible flow solvers using unstructured grids. Rapports de Recherche 1732, INRIA, 1992.

[10] E.D. Fernández-Nieto. Aproximación numérica de leyes de conservación hiperbólicas no homogéneas. Aplicación a las ecuaciones de aguas someras. Tesis doctoral. Universidad de Sevilla, 2003.

[11] P. García-Navarro and M.E. Vázquez-Cendón. On numerical treatment of the source terms in the shallow water equations. *Comput. Fluids*, 29:951–979, 2000.

[12] A. Harten, P. Lax, and A. van Leer. On upstream differencing and Godunov-type schemes for hyperbolic conservation laws. *SIAM Rev.*, 25:35–61, 1983.

[13] M.E. Hubbard and P. García-Navarro. Flux difference splitting and the balancing of source terms and flux gradients. *J. Comput. Phys.*, 165:89–125, 2000.

[14] R.J. LeVeque. *Finite Volume Methods for Hyperbolic Problems*, volume 31 of *Cambridge Texts in Applied Mathematics*. Cambridge University Press, 2002.

[15] P.M. Lloyd and P.K. Stansby. Shallow water flow around model conical islands of small side slope. Part 1: Surface piercing. *J. Hydraul. Eng.*, 123:1057–1067, 1997.

[16] L. Pena, L. Cea, and J. Puertas. Turbulent flow: An experimental analysis in vertical slot fishways. In *Fifth International Symposium on Ecohydraulics, Madrid, Spain*, pages 881–888. IAHR, 2004.

[17] J. Puertas, L. Pena, and T. Teijeiro. An experimental approach to the hydraulics of vertical slot fishways. *J. Hydraul. Eng.*, 130(1):10–23, 2004.

[18] A.K. Rastogi and W. Rodi. Predictions of heat and mass transfer in open channels. *Journal of the Hydraulics Division*, HY3:397–420, 1978.

[19] P.L. Roe. Discrete models for the numerical analysis of time-dependent multidimensional gas dynamics. *J. Comput. Phys.*, 63:458–476, 1986.

[20] E.F. Toro. *Riemann Solvers and Numerical Methods for Fluid Dynamics. Second Edition.* Springer-Verlag, New York, 1999.

[21] E.F. Toro. *Shock-capturing Methods for Free-Surface Shallow Flows.* Wiley, Chichester, West Sussex PO19 1UD, England, 2001.

[22] M.E. Vázquez-Cendón. An efficient upwind scheme with finite volumes of the edge-type for the bidimensional shallow water equations. In F. Benkhanldoun and R. Vilsmeier, editors, *Finite Volumes for Complex Applications. Problems and Perspectives*, pages 605–612. Hermes, 1996.

[23] M.E. Vázquez-Cendón. Improved treatment of source terms in upwind schemes for the shallow water equations in channels with irregular geometry. *J. Comput. Phys.*, 148:497–526, 1999.